On the high creep strength of the W containing IRIS-TiAl alloy at 850°C

Alain Couret, Jean-Philippe Monchoux, Daniel Caillard

On the high creep strength of the W containing IRIS-TiAl alloy at 850°C

*Alain Couret *, Jean-Philippe Monchoux and Daniel Caillard*

CEMES, Université de Toulouse, CNRS, 29 rue Jeanne Marvig, 31055 Toulouse, France

* Corresponding author: alain.couret@cemes.fr

Abstract

This paper presents a study of the creep at 850°C under 150 MPa of the IRIS alloy (Ti-Al48-W2-B0.1) densified by spark plasma sintering. The dislocation microstructure in a sample strained up to 1.5% was studied by post-mortem transmission electron microscopy. The deformation is mainly due to ordinary dislocations. Several populations of dislocations are evidenced. Their Burgers vectors, the plane in which they are moving and the corresponding deformation mechanisms are determined. In the discussion section, the deformation mechanisms, the factors controlling their activation and the role of tungsten as hardening element are examined.

Keywords

Titanium aluminides; Creep; Dislocations; Transmission Electron Microscopy; Glide and Climb

1. Introduction

TiAl intermetallic alloys [1] developed for high temperature structural applications in aeronautic and automotive industries are multiphase alloys, associating γ, α_2 and sometimes β_0 phases. However, the plastic deformation is mainly concentrated in the γ phase which is ordered into the quadratic $L1_0$ structure. Whatever the temperature and the deformation conditions, the main deformation modes in the γ phase involve ordinary dislocations (Burgers vector: 1/2<110]), which are similar to the dislocations in f.c.c. metals. Twinning and more scarcely other families of dislocations can also be activated as secondary systems because of the limited number of ordinary dislocation families in the structure.

At low temperatures (20°C to ~ 400°C), ordinary dislocations observed in the transmission electron microscope (TEM) are elongated along their screw orientation and anchored at many pinning points [2-4]. The corresponding glide process in (111) plane is controlled by a periodic frictional force of Peierls type, which has been associated to a non-planar core spreading [4]. The pinning points were controversially ascribed to either intensive cross-slip [2,3], or to small clusters due to local chemical segregations [5]. However, the observation of the same pinning points with the same density on twinning Shockley dislocations has been considered as a proof of the second explanation because Shockley dislocations are not able to cross-slip in nature [5]. At intermediate temperatures (400°C – 600°C), plastic instabilities were measured during

tensile tests [6] and ordinary dislocations were observed to move by a very fast and sudden movement of bursts of numerous dislocations which are in their screw orientation at the end of this process [7]. This behaviour has been attributed to dynamic strain ageing [7,8] and correlated to the yield stress anomaly measured in single γ crystals [6,9]. At higher temperatures (around 700°C), climb of dislocations was evidenced by in situ experiments performed in a transmission electron microscope [10,11], in consistency with the measurements of an activation energy during tensile tests close of the self-diffusion energy in γ TiAl alloys [11]. At 750°C during creep, ordinary dislocations have been evidenced to move by a mixed climb mechanism, for which the plane of motion is close to but distinct from the glide plane [12]. At temperatures above 800°C, the behaviour of ordinary dislocations is poorly documented except in the work of Kad and Fraser who showed that, at 900°C, a decrease of the strain rate promotes the activation of climb instead of glide [13]. This activation of climb is associated to the the brittle to ductile transition by several authors [1,11,13]. At 1 000°C, in aluminum rich single crystals, Inui *et al.* have observed the glide of ordinary dislocations in non-compact planes, as (001) and {110) planes [14] and Whang *et al.* the activation <010] dislocations in the (001) plane [15].

Concerning the creep properties, in particular at 800°C-850°C, there is still uncertainty on the nature of the deformation process carried by the ordinary dislocations, but it is well-known that addition of elements as Nb, Mo, Ta, Zr or W is a successful route to improve the alloy strength. For instance, in a recent systematic study performed in fully lamellar TiAl alloys containing 5% at. of Nb, Ta and Zr, Bresler et *al.* [16] have demonstrated that, at 900°C, this hardening effect is resulting from solid solution hardening but also from the low diffusivity and solubility of these species in the γ phase. The influence of incorporated tungsten atoms on the creep properties has been investigated in several studies (see for example references [17-23]), in particular in that dedicated to the alloys of the ABB family [19,20] and in that from the Otawa group [17,18]. All these works mainly consider that tungsten atoms modify the alloys properties through the formation of β/β_0 phase. That might be detrimental to the alloy strength due to the formation of β/β_0 grains easily deformable at high temperature. Or conversely, thatmight increase the alloy strength or thermal stability by an interfacial precipitation. Additionally, interfacial β/β_0 precipitates have been observed to hinder the interface dislocation emission and motion [17,18]. Finally, Seo *et al.* [18] speculated that the W atoms present in the γ phase could reduce the mobility of gliding dislocations and consequently increase the non-conservative dislocation motion.

In this context, the present paper will pay attention to the behavior of ordinary dislocations in a IRIS-TiAl alloy [24,25] crept in tension at 850°C under 150 MPa. The IRIS alloy, with a chemical composition of Ti-Al48-W2-B0.1, was densified by Spark Plasma Sintering (SPS). Its microstructure is consisting of small lamellar grains (~ 40 µm) surrounded by γ zones, called hereby γ borders, of about 5 µm width in average. More generally, the goal of this paper is to propose an explanation of the creep properties of the IRIS alloy at 850°C and a deeper understanding of the hardening effect of tungsten.

2. Experimental

The material used in the present work is a IRIS-TiAl alloy which was densified by Spark Plasma Sintering using a pre-alloyed powder (Ref A1261) atomised by the ATI company (Pittsburgh, PA, USA). The real composition of the powder was Ti49.9-Al48.0-W2.-B0.1. The SPS experiments were performed at the PNF2 (Plateforme Nationale de Frittage Flash/CNRS of

Toulouse, France). Following the classical SPS cycle described elsewhere [26], the true temperature of the material during the plateau was 1 350°C. The diameter and the height of the billets were 36 mm and 8 mm, respectively.

Creep tests under constant tensile loading were carried out in air, in an Adamel machine, at 850°C [27]. Strain was measured with Linear Variable Displacement Transducer extensometers (LVDT), which are in contact with the sample extremities. The displacement resolution was 1 µm and the time resolution 5s. Temperature was controlled in three points by K thermocouples, located in top, middle and bottom of the samples. The temperature gradient was less than 5°C along the sample. Three creep samples with a gauge section of 2.2 mm and a gauge length of 10 mm were cut in the SPS billets. The TEM observations were performed on thin foils extracted from a sample crept at 850°C, under 150 MPa, till 1.5% of plastic strain.

The TEM specimens were cut in the material with the loading axis either perpendicular, or parallel to the thin foil plane. 17 γ grains of borders and 5 lamellar zones were investigated. 12 of the 17 grains were situated in three thin foils cut perpendicular to the loading axis. The other five were situated in two thin foils containing this axis. To determine in which plane and by which process the dislocations are moving, tilt experiments have been conducted. Using a tilt-rotation specimen holder, the dislocation loop is firstly oriented with its two extremities parallel to the holder tilt axis, which is vertical on the TEM screen and micrograph. The goal of these experiments is to turn around the trace of the loop plane, which is the intersection of this plane with one surface, and to measure the variation of the apparent width of the loop. If the plot follows a sinusoidal variation, the loop plane can be determined from its extremums with the help of the stereographic projection. The experimental uncertainty on this kind of measurement is considered to be of ±5°. The success of this kind of experiment is conditioned by the location of these two extremities on the same thin foil surface. If that is not the case, namely if the two extremities belong to the two different surfaces, the subsequent tilts will not allow to turn around the trace of the loop plane. Another origin of failure could be that the loop segments are situated in several planes, for example as a result of the activation of cross-slip.

3. Creep curves

Fig. 1 shows two creep curves obtained at 850°C under 150 MPa. One experiment (red curve) was conducted to the failure of the sample whereas the second one (blue curve) was interrupted at 1.5% of plastic strain to observe the dislocation microstructure resulting from the first creep stages. Under this solicitation, the minimum creep rate was 6. 10^{-8} s^{-1}, and the creep life 260 h. The durations to reach 0.2, 0.5 and 1% of plastic strain were 0.15 h, 1.86 h and 13h, respectively.

It is always difficult to compare results of creep experiments to literature data, since the different authors take various solicitations. That is particularly true for experiments at 850°C. Nevertheless, using the Larson-Miller plot at a strain of 1% built by Appel *et al.* [1, Fig. 9.26], the behaviour of the IRIS alloy can be compared to other TiAl alloys. A duration of 13h at 850°C under 150 MPa lead to a value of 23.7 for this parameter, which attests of a high creep strength. For instance, in this Appel's graph, the values reported for TiAl alloys for a stress of 150 MPa range between 21.3 and 23.6.

4. TEM studies of ordinary dislocations

Ordinary dislocations were observed in all of the 17 investigated γ grains. However, they were detected in two configurations which will be successively described in the following sections.

4. 1 Gliding dislocations

On Fig. 2 (a&b), ordinary dislocations (marked A to C) are clearly elongated in the direction of their Burgers vector $1/2[\bar{1}\bar{1}0]$ and connected to smoothly curved non-screw segments at the extremities of the screw ones (view b). Since the $(1\bar{1}1)$ plane is upright on view a, the straight-lined aspect of the dislocations indicates that they are confined in this $(1\bar{1}1)$ plane, which is a glide plane since it contains the Burgers vector. These dislocations have thus moved by glide in this plane.

A few shorter dislocations which do not exhibit this elongated shape are noted 1 to 5. Using the $\boldsymbol{g}.\boldsymbol{b} = 0$ criterion, the Burgers vector of these dislocations has been verified to be also $1/2[\bar{1}\bar{1}0]$. Their rectilinear aspect and the nearly alignment of their two extremities on view (a) indicate that they are also lying in the $(1\bar{1}1)$ glide plane. Since, the $(1\bar{1}1)$ plane is inclined at 55° with respect to the thin foil plane, and since the $[\bar{1}\bar{1}0]$ screw direction is nearly parallel to the foil plane, these non-screw segments are widely inclined with respect to the thin foil plane. Because of this pronounced inclination, the observation of many of them demonstrates that they are quite long, otherwise the probability that they are in the thin foil and, so visible, would be very low.

Fig. 2,c to e shows in the same γ grain several of these $1/2[\bar{1}\bar{1}0]$ dislocations (marked D to G) interacting with a tilt sub-boundary. The dislocation marked D is likely to enter the sub-boundary. Since this incorporation process requires a diffusion assisted rearrangement of the sub-boundary, this confirms that all the above straight screw dislocations have appeared during the creep deformation at elevated temperature. Therefore, it rules out the possibility of the above glide process to be an artefact resulting from the sample cooling or the thin foil preparation.

On views Fig. 2b & c, arrows indicate some anchoring points on screw and non-screw segments. They look similar to those observed in TiAl alloys deformed at low temperatures [2-5].

Fig. 3 shows a grain crossed by twins situated in (111) and $(\bar{1}11)$ planes. Curved ordinary dislocations with the two available Burgers vectors are observed, namely $b_1=1/2[\bar{1}10]$ for dislocation marked d_1 and $b_2=1/2[110]$ for dislocations marked d_2 & d_3. Tilt experiments have been performed on these three dislocations, in order to determine their corresponding planes of motion. The apparent width of dislocation loops d_1 and d_2 does not follow a sinusoidal variation as a function of the tilt angle, rendering the determination of their plane impossible, as explained in section 2. Fig. 4 displays the dislocation d_3 under different inclinations. The precaution was taken to measure the width using positive and negative diffracting vectors (not reproduced here), with similar deviations to the Bragg's angle and to take the average value. This average apparent width is plotted as a function of the tilt angle in Fig. 4 (g). The corresponding plot follows part of a sinusoidal variation, from which the loop plane could be determined with the help of the stereographic projection. On the stereographic projection of the grain (Fig. 4 (h)), the pole of the loop plane is marked P (marked in green), with a trace reported in green. This plane appears to be the (002) plane which is a non-close-packed glide plane for the ordinary dislocations. Surprisingly, the corresponding system ($1/2[110]$ in (002) plane) has a low Schmid factor (0.12), indicating that its activation does not accommodate the applied strain. This observation is very similar to those of Inui et al. [14] who have observed ordinary dislocations in the (002) plane in a [001] oriented Al rich alloy deformed at 1 000°C. These authors claimed that this (002) glide is activated to release internal stresses resulting from twin/twin intersections as observed at room temperature [28,29]. In the present case, a twin/twin

intersection has been observed in this grain but the correlation between this intersection and the studied dislocations has not been established. However, it is probable that the activation of this glide in (002) plane is resulting from internal stresses. On Fig. 4,d where the (002) plane is nearly parallel to the observation plane, it can be seen that one dislocation segment is close to screw direction of the dislocation $1/2[110]$.

As a conclusion, gliding ordinary dislocations have been observed after high temperature creep. As at lower temperatures, when gliding in the {111} type plane, these dislocations exhibit rectilinear screw segments anchored at some pinning points. However, contrary to what has been observed at lower temperatures, long non-screw segments have also been observed. One event of glide in a (002) plane has also been reported.

4.2. Climb in closed packed planes

Figs. 5 and 6 show ordinary dislocations in two different γ grains of two thin foils cut perpendicularly to the tensile axis of the crept specimen. Their long apparent length indicates that they are situated close to the foil plane.

In the first case (Fig. 5), the Burgers vector of the dislocations is $1/2[\bar{1}10]$ making an angle of 52° with the thin foil plane. Numerous tilt experiments around various directions were performed on these dislocations to determine the plane in which they are lying. Fig. 7 shows one of them over the zone surrounded by the blue rectangle on Fig. 5a, with the tilting axis parallel to the rectilinear segments. The dislocations not parallel to the rectilinear segments are divided into several parts, called macro-jogs, which are assumed to result from a displacement in a single plane. The apparent height of four of them (M1 to M4) were measured on each view. The results are reported as a function of the tilt angle (Fig. 7 (h)). Weak variations were detected but it seems that the maxima are close to zero tilt confirming a moving plane close to the thin foil plane. This shows that dislocations have moved in the foil plane perpendicular to the straining axis.

For the second case (Fig. 6),dislocations with $b_1 = 1/2[\bar{1}10]$ and $b_2 = 1/2[110]$ Burgers vectors are observed together. Remarkably, a b_1 and a b_2 dislocations are nearly parallel to the same direction ($[\bar{1}0\bar{1}]$), indicating that the ordinary dislocations can align in various close-packed directions independently of their Burgers vector. Tilt experiments around different directions have shown that these dislocation loops are in a plane perpendicular to the tensile axis. A few shorter b_1 dislocations are also visible; they are screw oriented and have probably moved by glide as described in section 4.1.

Considering the orientation of these two grains, it is thus probable that the dislocations are lying in closed-packed planes situated perpendicularly to the tensile axis namely in $(\bar{1}11)$ and (010) planes for the case of Figs. 5 and 6, respectively. Since these planes are far away from all slip planes containing the corresponding Burgers vectors, it appears that the movement of these dislocations involves a large climb component. For the recording of these two micrographs, the zone axis normal to these $(\bar{1}11)$ and (010) planes have been placed parallel to the electron beam to have the corresponding planes strictly parallel to the observation plane. In both grains, the long dislocations are oriented close to closed packed directions of <101] type, however not exactly. Other examples of similar configurations have been found with sometimes a climb plane of {101) type (systems C1 and C3 in Tab. 1). It is worth to note that pure climb of [001]

dislocations with similar shape has been previously observed in the same IRIS alloy crept in the same conditions [30].

Fig. 8 provides more details about the structure of these dislocations. This figure shows the zone of Fig. 5 under two inclinations achieved by a rotation around the direction of the long dislocations [101]. Let us recall that the main plane containing the observed dislocations with Burgers vector $1/2[\bar{1}10]$ is the climb plane $(\bar{1}11)$. Two important points are to be noted. First, rectilinear segments parallel to [101] marked by arrows in Fig. 8 (a) appear curved on view (b). Since the $(\bar{1}\bar{1}1)$ plane is upright in 8(a), not in 8(b), this indicates a movement in the $(\bar{1}\bar{1}1)$.plane which is a slip plane for $1/2[\bar{1}10]$ dislocations. Second and conversely, for the dislocations aligned along $[01\bar{1}]$ direction and surrounded in black, those surrounded in dashed line are curved on the view (a), demonstrating a short range motion in the (111) plane, which is also a slip plane. Note that some dislocations of the same family (surrounded in full line) remain rectilinear whatever the inclination. Moreover, some pinning points, which are considered to be typical of a glide process, are clearly visible on these curved dislocations. These observations thus indicate that non-screw dislocations moving mainly by climb can also deviate and slip in intersecting {111} glide plane, apparently over short distances. Such a deviation has been observed in several thin foils for sixty degrees oriented ordinary dislocations.

As a conclusion, the main features of these dislocations are to lie in planes perpendicular to the tensile axis and to be elongated along the closed packed directions of <101] type. Their motion thus involves a large component of climb. They are however able to cross-slip in intersecting {111} type glide planes.

4.3. Deformation microstructure in lamellar areas

Fig. 9 illustrates that the deformation of lamellar zones occurs by the same processes as in the γ borders. We have performed similar TEM analyses to those presented above with the aim to determine their moving processes (not detailed here). On view (a), some gliding rectilinear screw ordinary dislocations are anchored at many pinning points (see the enlargement). In view (b), climbing ordinary dislocations are observed; many of them are attached to the interface where they have been nucleated. This kind of climbing dislocations has been attributed to the emission of interfacial dislocations during the primary creep [10,11]. The pinning of climbing dislocations has been shown to be more efficient in the W-containing alloys due to β/β_0 precipitation at lamellar interfaces [17,18]. Twins crossing interfaces are observed in view (a) ; they are more numerous in lamellar zones than in γ grains.

5. Discussion

In the present work, the dislocation microstructure resulting from the creep of the IRIS alloy at 850°C under 150 MPa has been investigated in 17 γ grains of the borders. In all of them, ordinary dislocations have been observed. In some grains, ordinary dislocations with the two existing Burgers vectors have been observed together. These dislocations are observed in two configurations which have been attributed to glide and climb deformation processes respectively. Determining which one of these two processes is operative for all the activated Burgers vectors is a difficult task, which is moreover not always possible owing to unsuitable thin foil orientation and to the insufficient tilt capacity of the microscope. Tab. 1 presents the features of 11 systems for which the corresponding deformation process has been determined. Note that 5 glide and 6 climb configurations have been unambiguously evidenced. They were

observed in both perpendicular (TFP1, TFP2 and TFP3) and longitudinal (TFL4 and TFL5) thin foils. In Fig. 10, the orientations of the grains have been situated and discriminated as a function of the activated process in a unit standard triangle adapted to the $L1_0$ structure. These table and figure illustrate a moderate dependence of the activated system on the stress orientation which will be discussed in more details below.

Glide configurations made of long rectilinear screw dislocations anchored at small pinning points have been observed in the present work, as previously seen in the γ phase of TiAl alloys in a large range of temperature [2-7,13]. The anchoring on small pinning points is thus present in the whole range of temperature, which is consistent with the fact that they are due to local chemical segregations [5]. The minimum value of the Schmid factor for the activation of glide is of the order of 0.2-0.3 (Systems G1 to G5 in Tab. 1). On the one hand, as at low temperatures, the gliding dislocations are clearly elongated along their screw orientation at 850°C (Fig. 1) indicating that a frictional force acting on screw segments is still present and rate-controlling. Consistently with the strictly rectilinear aspect of some screw segments (Figs. 1 and 8), the frictional force is probably resulting from the non-planar core as at low temperature. On the other hand, in the intermediate temperature range (400°C-600°C) [7,8], a decrease of the frictional force has been observed, and a higher mobility of impurities has been deduced from the observation of dynamic strain ageing. It is thus probable that the strength of the high temperature frictional force results from the effect of the dragging force of solute atoms making a Cottrell atmosphere around dislocations (W in our case) on the Peierls-type friction stress originating from the non-planar core structure of screw segments. The corresponding mechanism has been detailed in the case of iron containing carbon in [31], where it has been shown that in the case of screw dislocations, an interaction between the non-planar core and mobile solute atoms may account for the observation of a Peirls-type friction stress at a high temperature where solute atoms are definitely mobile (i.e. above the temperature domain of dynamic strain ageing). The observation of non-screw rectilinear segments reveals their low mobility, which is not the case at lower temperatures and, which is also probably resulting from an interaction with the tungsten atoms.

Configurations resulting from a movement involving a large climb component have been observed in a high proportion of grains. The features of 6 climb systems are summarized in Tab. 1 (C1 to C6). It appears that the angle between the tensile axis and the Burgers vector $\widehat{\boldsymbol{b},\boldsymbol{T}}$ is widely distributed with an average value around 45°. It is interesting to note that the dislocations are climbing although their glide Schmid factor (GFS in Tab. 1) would be sufficient to activate glide, i.e. higher than the value of 0.2-0.3 found as the critical value for glide activation (precedent paragraph). What seems to be determining for the activation of this climb is the possibility for the dislocations to move in close-packed planes perpendicular to the tensile axis. It is of course made easier by the high temperature (850°C). The dislocation elongation along the closed-packed directions indicates that climb takes place by the slow and difficult nucleation of jog-pairs, followed by their faster lateral climb motion [32]. Due to this alignment, the climbing dislocations are able to cross-slip in intersecting {111} glide plane where they either glide over a short distance as observed, or they escape. Fig. 11 presents a sketch of this climb processes, designed according to the situation studied in the Figs. 5, 7 and 8. The dislocation shape in segments separated by macro-jogs (Figs. 5 and 6) is consistent with this movement by series of climb and glide events. This climb process in close packed planes perpendicular to the tensile axis is not different in nature from the mixed climb mechanisms

evidenced at 750°C [12]. In both cases, dislocation move by a non-conservative movement in a plane clearly different from the glide plane. The higher the temperature, the more pronounced is the deviation away from the glide plane, up to climb in a plane perpendicular to the tensile axis at 850°C.

That is probably the high temperature and the low stress level which lead to the coexistence of these two deformation mechanisms involving the same ordinary dislocations. Indeed, the high temperature facilitates the diffusion assisted climb whereas, despite this high temperature, the low stress level limits the activation of glide, which is difficult because of the efficiency of the frictional force enhanced by the presence of atoms of tungsten. The dispersion of the grain orientations for which glide and climb are observed (Fig. 10) indicates that the resolved applied shear stress which depends on the orientation of the grains with respect to the tensile axis is not the determinant parameter for the selection of the deformation modes. Consistently, Tab. 1 shows that the glide Schmid factor is not the pertinent data to explain the activation of glide. It is probable that, because of the low applied stress level, glide is operative under the effect of local internal stresses, as previously proposed for creep of a cast TiAl alloy [27,33]. In addition to the presence of a close-packed plane perpendicular to the tensile axis, a favourable orientation of the grain with respect to the loading axis, materialised by a high value of the climb Schmid factor (CSF in Tab. 1) seems to promote the activation of climb.

The creep strength of the lamellar zone is associated to the interaction between the mobile dislocations and the γ/γ and γ/α_2 interfaces [1]. For the case of glide, our TEM observations show that these interaction processes are probably similar to those observed at room temperature [34,35], for which transmission processes of the deformation are operative in favourable crystallographic conditions under the effect of stress concentration resulting from pile-up effects. These processes of interface crossing are probably the reason of the more important activity of twinning in γ lamellae than in γ borders, since switches between gliding ordinary dislocations and twin have been frequently observed at γ/γ interfaces. On the reverse, when ordinary dislocations are moving by climb, direct interface crossing seems to be not operative, probably because of a lack of stress concentration, in such a way that dislocations sources at interfaces seems to be more efficient [1,11]. The higher resistance of lamellar zones is probably correlated to the confinement of the deformation in the lamellae. The moving dislocations might incorporate in interfaces and annihilate, here again through diffusion assisted processes.

Interestingly, glide and climb occur by the nucleation and the lateral propagation of a pair of short dislocation segments, namely kinks for glide and jogs for climb. The corresponding elementary steps are thus described by similar critical configurations made of pairs of kinks or jogs. Hence, similar stress dependences are expected for these two mechanisms, characterised by the stress exponent or the activation volume. In particular, the activation volume is directly correlated to the area swept by the dislocation when it reaches these critical configurations. This explains satisfactorily the high measured values of the activation volume which is of the order of 40-50 b^3 [10-12], i.e. larger than those expected for a pure climb mechanism (a few b^3). Provided that they are isolated and randomly distributed in the γ phase, the addition of tungsten atoms reduces the dislocation mobility in both cases through core or elastic interactions depending on the character and core structure of dislocations. The displacement of these tungsten atoms will control the dislocation mobility for both glide and climb and consequently the creep properties through their low diffusivity. Consistently, the creep activation energy of

TiAl alloys is measured between 300 kJ/mol and 400 kJ/mol depending on microstructures and chemical compositions which is in the range of the self-diffusion energies of the species [1]. In the W and B containing ABB-23 alloy, Lapin *et al*. [20] have measured an activation energy of 355 kJ/mol, which they have interpreted as a signature of dislocation climb as rate controlling mechanism. Interestingly, this confirms that the creep is rather controlled by the motion of ordinary dislocations than by the secondary systems which have to be activated, as twinning on motion of other types of dislocations. In addition to its positive effect on the microstructure and alloy strength at high temperature, the incorporation of tungsten has been assumed to enhance the creep properties by reducing directly the dislocation mobility in the γ phase [18].

After the successful implementation of TiAl alloys in blades of the last stages of the low pressure turbines of aircraft engines, a working temperature range around 800°C is now targeted for both aeronautic and automotive applications, with a special attention to creep, fatigue and ageing properties. The present work has shown that climb and glide controlled by the dragging of solute atoms are in competition in this targeted temperature range. In both cases the atoms of tungsten are assumed to reduce the dislocation mobility because of their low diffusivity. More generally, the current literature shows that other elements with relative low diffusivity like Nb, Mo, Ta or Zr … [1] also increase the creep strength, probably through the same process. However, the use of tungsten as additive element, with an amount of 2at. % in the IRIS alloy, presents a strong advantage correlated to its very low diffusivity. Indeed, a high aluminium content can be preserved in the alloy, which reduces the presence of α_2 and β_0 phases, which are detrimental to the room temperature ductility and to the high temperature strength of the alloy, respectively. In addition, Spark Plasma Sintering permits the mastering of a random distribution of tungsten atoms in the γ phase of both single-phased and lamellar zones, by the control of its thermal cycle which avoids a remelting of the alloy which would lead to tungsten segregation.

Summary

During creep of the IRIS alloy at 850°C and 150 MPa, the deformation occurs mainly by ordinary dislocations, which move by glide or by a process involving a large climb component. The gliding dislocations are rectilinear along their screw orientation and anchored at many pinning points. Glide is controlled by a frictional force resulting from the non-planar spreading of the dislocation core, which is enhanced by the interaction between the dislocation and the tungsten atoms. The main features of the climbing dislocations are to move in planes which are perpendicular to the tensile axis and to be elongated along close-packed directions of <101] type. This mechanism which occurs by the nucleation and propagation of pairs of jogs is controlled by diffusion of tungsten atoms. Because their critical configurations are made of pairs of dislocation segments in the moving plane (kinks or jogs), the high value of the stress dependence for creep, in particular the activation volume, is reasonably explained by the occurrence of these two mechanisms. The high creep resistance of the IRIS-TiAl alloy is ascribed to the presence of tungsten atoms in the γ phase and to their low diffusivity. The spark plasma sintering route allows to control their repartition in the γ phase of the borders and lamellae, and to avoid their precipitations in the β_0 and α_2 phases.

Acknowledgements

The authors want to thank the Université Fédérale – Toulouse Midi-Pyrénées for supporting the project “ALTIAERO” of the “IDEX-ATS” program during which this work was conducted.

References

[1] F. Appel, J. Paul, M. Oehring: *Gamma Titanium Aluminides : Science and Technology, © Wiley-VCH Verla GmbH &Co. KGaA*, 2011.

[2] S. Sriram, D.M. Dimiduk, P.M. Hazzledine, V.K. Vasudevan, The geometry and nature of pinning points of 1/2 (110] unit dislocations in binary TiAl alloys, Phil. Mag. A, 76 (1997) 965-993.

[3] B. Viguier, K.J. Hemker, J. Bonneville, F. Louchet, J.L. Martin, Modeling the flow stress anomaly in gamma TiAl. 1. Experimental observations of dislocation mechanisms, Phil. Mag. A, 71 (1995) 1295-1312.

[4] A. Couret, An in situ study of ordinary dislocations glide in TiAl alloys, Phil. Mag. A, 79 (1999) 1977-1994.

[5] S. Zghal, A. Menand, A. Couret, Pinning points anchoring ordinary and Shockley dislocations in TiAl alloys, Acta Mat., 46 (1998) 5899-5905.

[6] F. Grégori F, Plasticité de l'alliage γ-TiAl : rôle des dislocations ordinaires et superdislocations dans l'anomalie de limite d'élasticité, *Ph D Thesis* Université de Paris VI, 1999.

[7] G. Molénat, A. Couret, D. Caillard. Peierls friction stresses and dynamic strain ageing in TiAl and Fe30% Al alloys, Material Science and Engineering 234-236 (1997) 660-663.

[8] D. Haussler, M. Bartsch, M. Aindow, I.P. Jones, U. Messerschmidt, Dislocation processes during the plastic deformation of gamma-TiAl, Phil. Mag. A, 79 1999, 1045-1071.

[9] T. Kawabata, T. Kanai, O. Izumi O, Positive temperature depence of the yield stress in TiAl $L1_0$ type superlattice intermetallic compound single-crystals at 293-1273K, Acta Metall. Mater, 33 (1985) 1355-1366.

[10] F. Appel, U. Lorenz, M. Oehring, U. Sparka, R. Wagner, Thermally activated deformation mechanisms in micro-alloyed two-phase titanium aluminide alloys, Materials Science and Engineering A 233 (1997) 1-14.

[11] F. Appel, R. Wagner Microstructure and deformation of two-phase gamma-titanium aluminides, Materials Science and Engineering: R: Reports 22 (1998) 187-268.

[12] J. Malaplate, D. Caillard, A.Couret, Interpretation of the stress dependence of creep by a mixed climb mechanism in γ-TiAl Phil. Mag. A, 84 (2004) 3671-3687.

[13] B.M. Kad, H.L. Fraser, On the contribution of climb to high-temperature deformation in single phase gamma –TiAl, Phil. Mag. A, 69 (1994) 689-699.

[14] H. Inui, M. Matsumuro, D.H. Hu, M. Yamaguchi, Temperature dependence of yield stress, deformation mode and deformation structure in single crystals of TiAl (Ti-56 at% Al) Phil. Mag. A, 75 (1997) 395-423.

[15] S.H. Whang, Y.D. Hahn, Positive temperature dependence of the yield stress in $L1_0$-type Ti-Al-V compound, Scripta Metallurgica and Materiala, 24, (1990) 485-490.

[16] J. Bresler, S. Neumeier, M. Ziener, F. Pyczak, M. Göken, The influence of niobium, tantalum and zirconium on the microstructure and creep strength of fully lamellar gamma/alpha(2) titanium aluminides, Mater. Sci. Eng. A, 744 (2019) 46-53.

[17] J. Beddoes, D.Y. Seo, W.R. Chen, L. Zhao, Relationship between tensile and primary creep properties of near gamma-TiAl intermetallics, Intermetallics, 9 (2001) 915-922.

[18] D.Y. Seo, J. Beddoes, L. Zhao, Primary creep behavior of Ti-48Al-2W as a function of stress and lamellar morphology, Metallurgical and Materials Transactions 31A, 10 (2003) 2177-2190.

[19] J. Lapin, M. Nazmy, Microstructure and creep properties of a cast intermetallic Ti-46Al-2W-0.5Si alloy for gas turbine applications, Mater. Sci. Eng. A, 380 (2004) 298-307.

[20] J. Lapin, Creep behavior of a cast intermetallic Ti-45.2Al-2W-0.6Si-0.7B alloy, Scripta Mat, 50 (2004) 261-265.

[21] A.M. Hodge, L.M. Hsiung, T.G. Nieh, Creep of nearly lamellar TiAl alloy containing W, Scripta Mat, 51 (2004) 411-415.

[22] M. Munoz-Morris, I. Gil, D.G. Morris, Microstructural stability of γ-based TiAl intermetallics containing β phase, Intermetallics, 13 (2005) 929-936.

[23] H. Zhu, D.Y. Seo, K. Maruyama, P. Au, Strengthening of a fully lamellar TiAl plus W alloy by dynamic precipitation of β phase during long-term creep, Scripta Mat, 54 (2006) 425-430.

[24] T. Voisin, J. P. Monchoux, M. Perrut, A. Couret A, Obtaining of a fine near-lamellar microstructure in TiAl alloys by Spark Plasma Sintering, Intermetallics, 71 (2016) 88-97.

[25] T. Voisin, J. P. Monchoux, C. Deshayes, M. Thomas, A. Couret, Mechanical properties of the IRIS TiAl alloy, Metallurgical and Materials Transactions 47A, 12 (2016) 6097-6108.

[26] T. Voisin, L. Durand, N. Karnatak, S. Le Gallet, M. Thomas, Y. Le Berre, J.F. Castagne, A. Couret A, Temperature control during Spark Plasma Sintering and application to up-scaling and complex shaping, Journal of Materials Processing Technology, 213 (2013) 269-278.

[27] J. Malaplate, M. Thomas, P. Belaygue, M. Grange, A. Couret, Primary creep at 750°C of $Ti_{48}Al_{48}Cr_2Nb_2$ alloys elaborated by powder metallurgy and cast processes, Acta Mat, 54 (2006) 601-611.

[28] Y.Q. Sun, P.M. Hazzledine, J.W. Christian, Intersections of deformation twins in TiAl. 1. Experimental observations. Phil. Mag. A, 68 (1993) 471-494.

[29] D. Wardle, I. Phan, G. Hug, Analysis of twin intersections in TiAl, Phil. Mag. A, 67 (1993) 497-514.

[30] S. Naanani, J. P. Monchoux, C. Mabru, A. Couret, Pure climb of [001] dislocations in TiAl at 850°C, Scripta Mat, 149 (2018) 53-57.

[31] D. Caillard and J. Bonneville, Dynamic strain ageing caused by a new Peierls mechanism at high temperature in iron, Scripta Mater 95 (2015) 15-18.

[32] F. Mompiou and D. Caillard, On the stress exponent of dislocation climb velocity, Mater. Sci. Eng. A483-484 (2008)143-147

[33] J. Malaplate, A. Couret, Study of creep at 750°C of Ti48Al48Cr2Nb2 alloys obtained by powder metallurgy and cast processes, Matériaux et Techniques, 1-2 (2004) 51-57.

[34] S. Zghal, A. Coujou, A. Couret, Transmission of the deformation through gamma-gamma interfaces in a polysynthetically twinned TiAl alloy - I. Ordered domain interfaces (120 degrees rotational), Phil. Mag. A, 81 (2001) 345-364.

[35] S. Zghal, A. Couret, Transmission of the deformation through gamma-gamma interfaces in a polysynthetically twinned TiAl alloy - II. Twin interfaces (180 degrees rotational), Phil. Mag. A, 81 (2001) 365-382.

	Systems	*Grains*	*TF*	*b*	$\widehat{b,T}$ (°)	*G SF*		*n (CP)*	$\widehat{n,T}$(°)	*C SF*
Glide	G1	Gr. 1	TFP1	$1/2[\bar{1}10]$	48	0.18				
	G2	Gr. 2	TFP1	$1/2[1\bar{1}0]$	46	0.3				
	G3	Gr. 3	TFL4	$1/2[110]$	86	0.2				
	G4	Gr. 4	TFL5	$1/2[110]$	35	0.3				
	G5	Gr. 5	TFL5	$1/2[\bar{1}\bar{1}0]$	64	0.35				
Climb	C1	Gr. 6	TFP1	$1/2[\bar{1}\bar{1}0]$	76	0.25		$(\bar{2}02)$	10	0.38
	C2	Gr. 1	TFP1	$1/2[\bar{1}10]$	46	0.18		$(1\bar{1}1)$	48	0.62
	C3	Gr. 7	TFP2	$1/2[1\bar{1}0]$	36	0.17		(202)	22	0.19
	C4	Gr. 8	TFP2	$1/2[\bar{1}10]$	50	0.4		(020)	3	0.64
	C5			$1/2[110]$	40	0.42		(020)	3	0.76
	C6	Gr. 9	TFL4	$1/2[110]$	35	0.31		$(\bar{1}00)$	16	0.66

Tab.1: summary of the features of the analysed systems. Grains: investigated grains, TF : thin foils (TFP and TFL for thin foils cut perpendicularly and parallel to the tensile axis, respectively), b : Burgers vectors, $\widehat{b,T}$: angles between the Burgers vectors and the tensile axes, GSF: highest glide Schmid factors of the two {111} glide systems involving this Burgers vector, n (CP): normals to the plane in which the dislocations are lying in case of climb, $\widehat{n,T}$: angles between this normal and the tensile axis and CSF: Schmid factors for this climbing system.

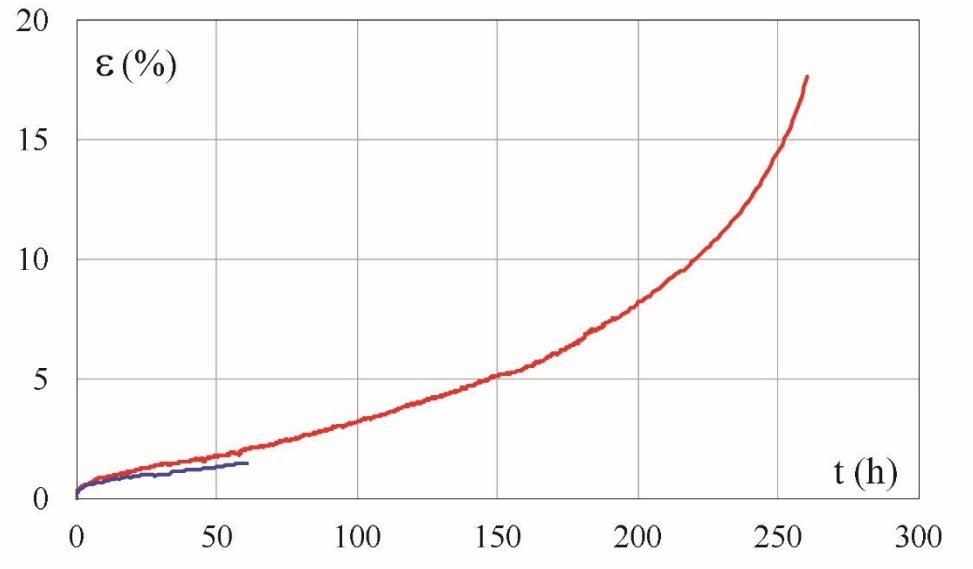

Fig. 1

Fig. 1 : Creep curves at 850°C under 150 MPa (red : till failure ; blue interrupted at 1.5% of plastic strain).

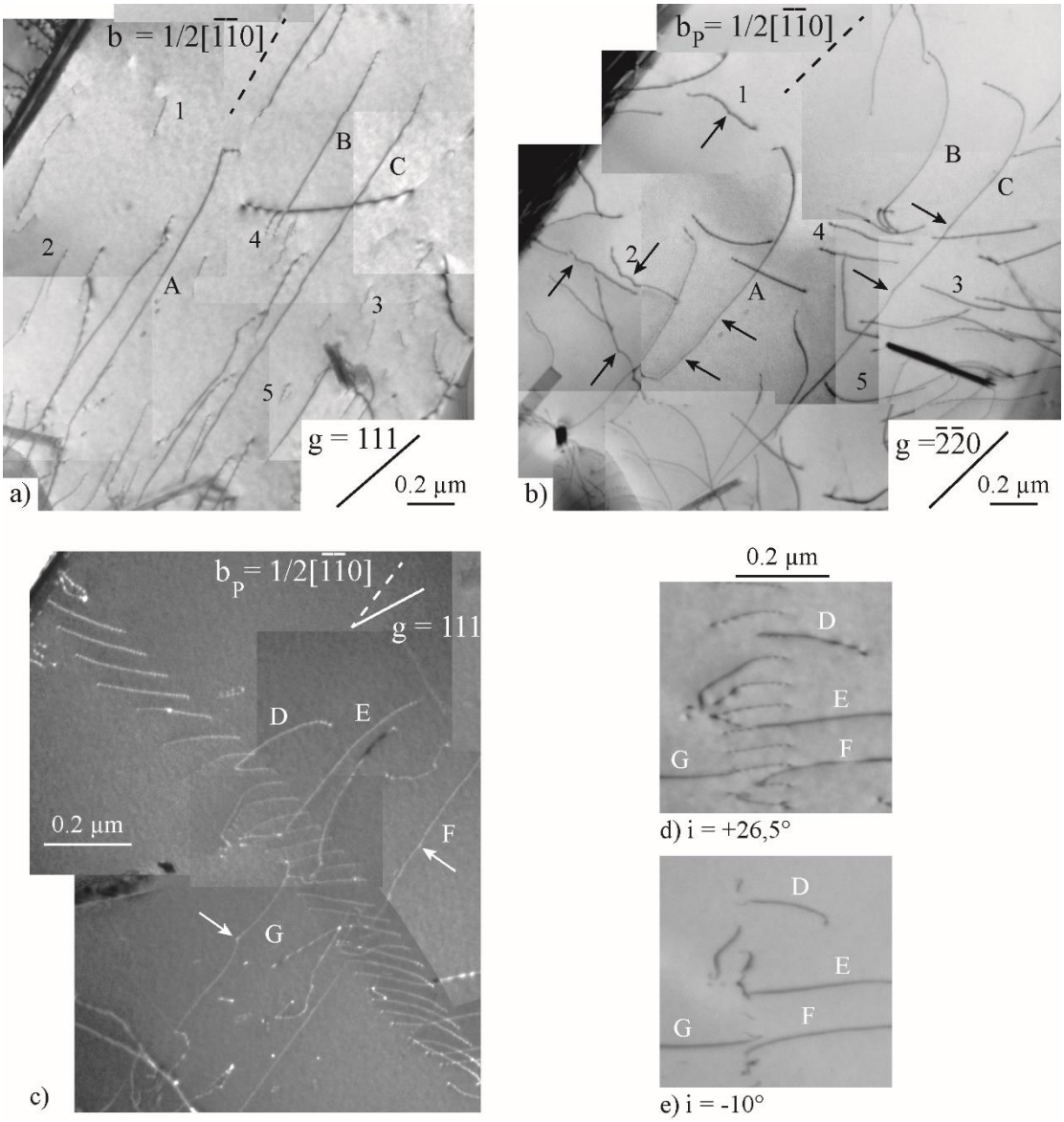

Fig. 2

Fig. 2: Gliding ordinary dislocations. (a) and (b): general views of screw elongated dislocations (marked A to C). Arrows indicate pinning points and numbers indicate short non screw dislocations. (c) to (e): interaction between gliding dislocations (D to G) and a flexion sub-boundary. Dislocation marked D is clearly incoming in the sub-boundary. b_P is the projection direction of the Burgers vector. (Thin foil: TFL5; Grain: 5).

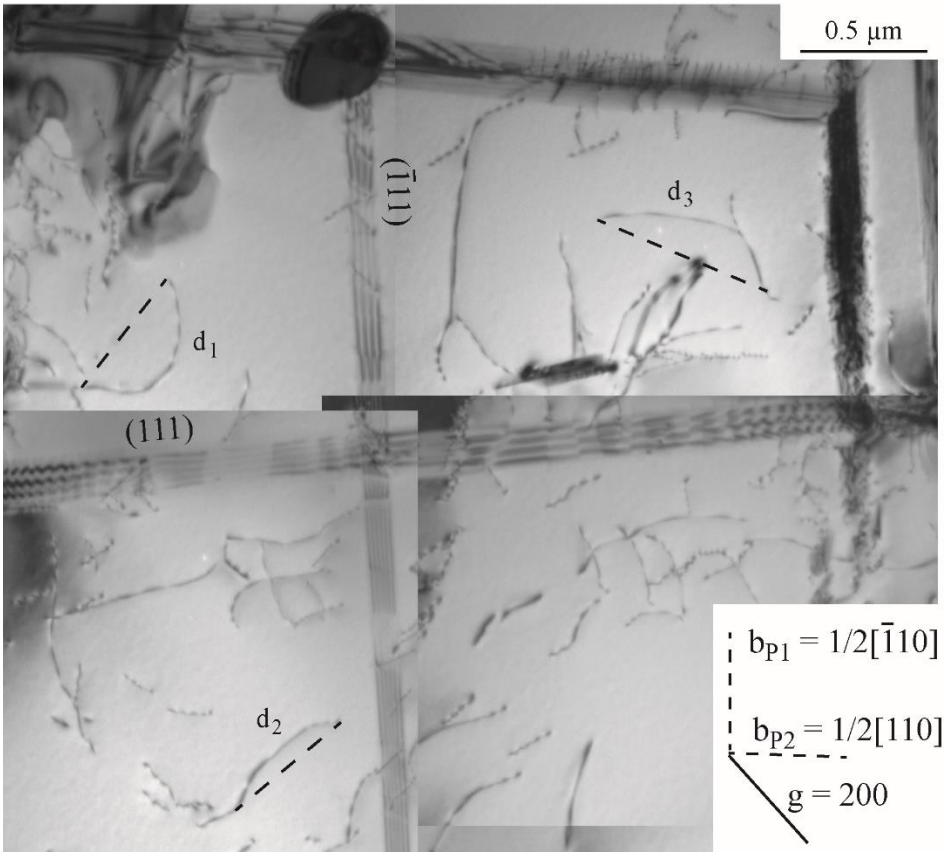

Fig. 3

Fig. 3: a γ grain containing twins in (111) and $(\bar{1}11)$ planes and ordinary dislocations with b_1 (d_1) and b_2 (d_2 and d_3) Burgers vectors. The loop plane of dislocations marked d_1 to d_3 has been studied by tilt experiments, dashed line indicating the direction around which the sample was tilted. b_P are the projection directions of the Burgers vectors. (Thin foil: TFP2; Grain: 14).

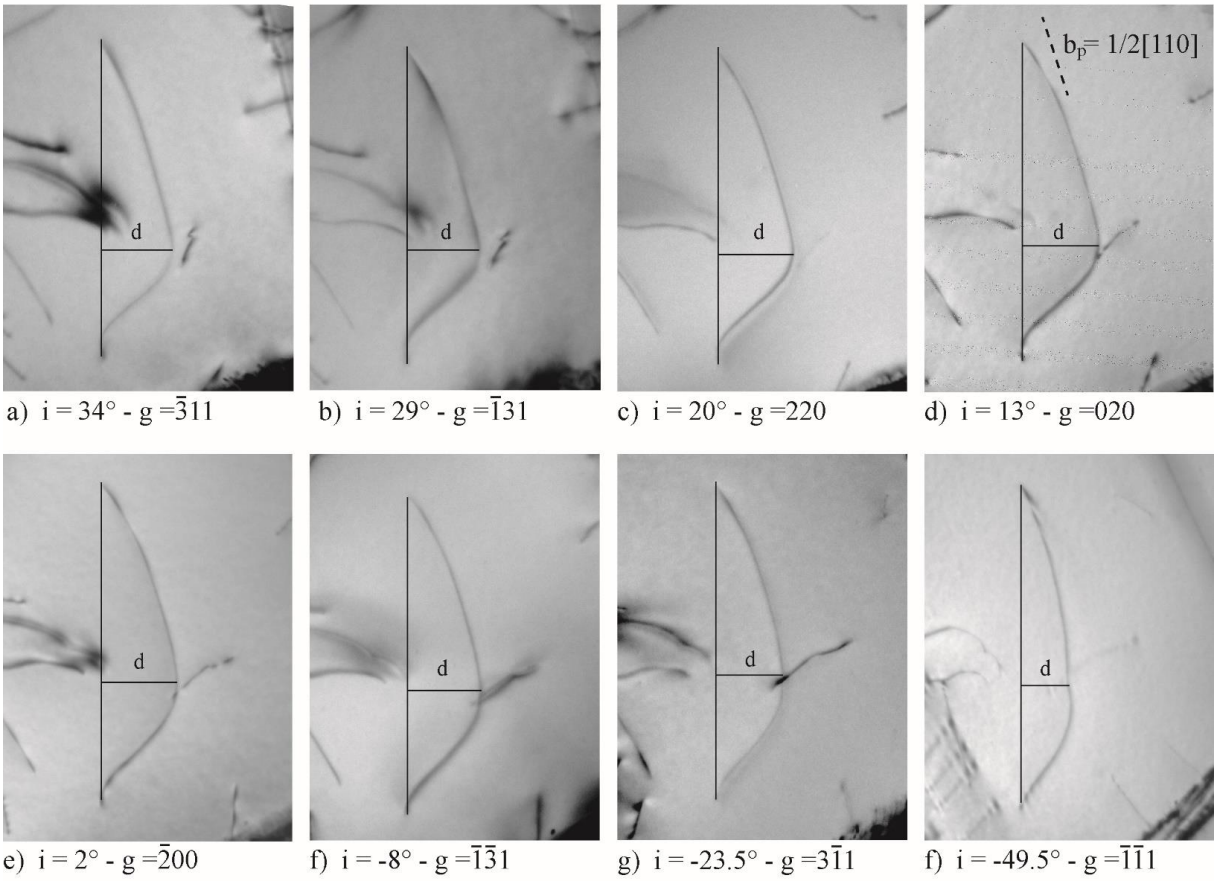

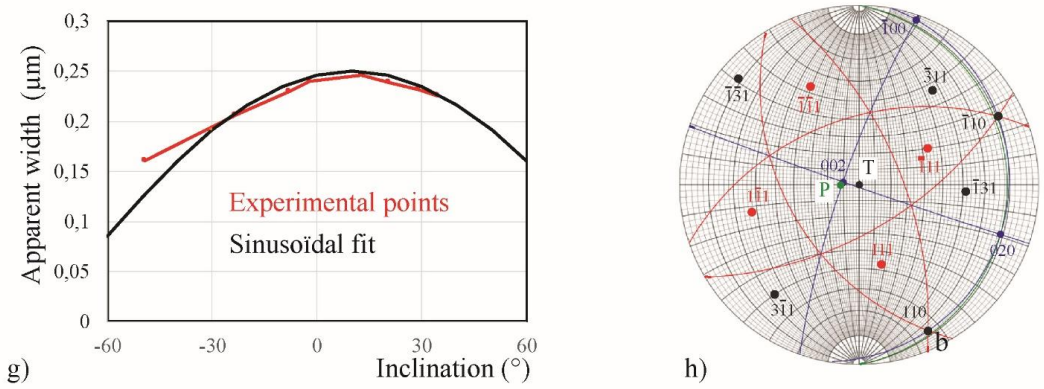

Fig. 4

Fig. 4: tilt experiment of the dislocation d_3 of Fig. 3. (a) to (f): micrographs under different inclinations. (g): variation of the apparent width with the inclination angle. (h): stereographic projection. b_P (view (d)) is the projection direction of the Burgers vector. (Thin foil: TFP2; Grain: 14).

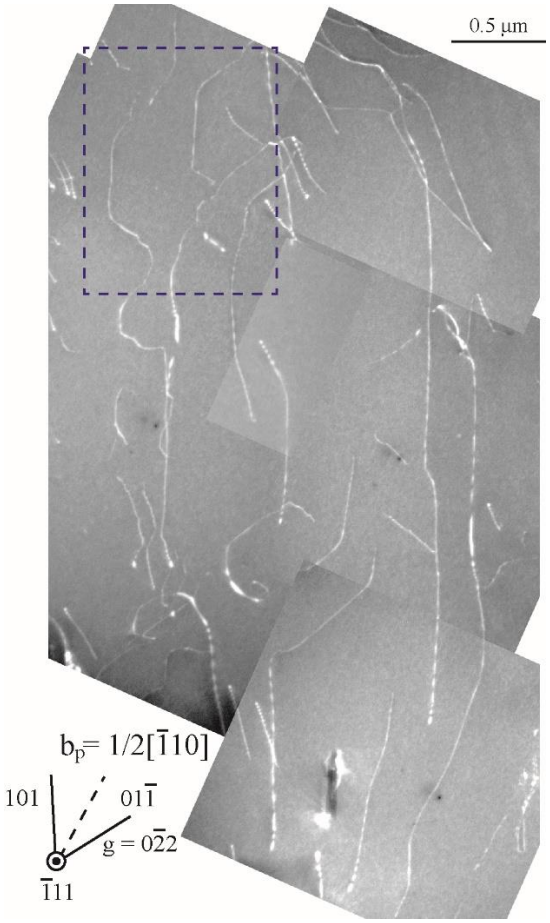

Fig. 5

Fig. 5: Ordinary dislocations in the $(\bar{1}11)$ plane perpendicular to the tensile axis of the crept sample. b_P is the projection direction of the Burgers vector. (Thin foil: TFP1; Grain: 1).

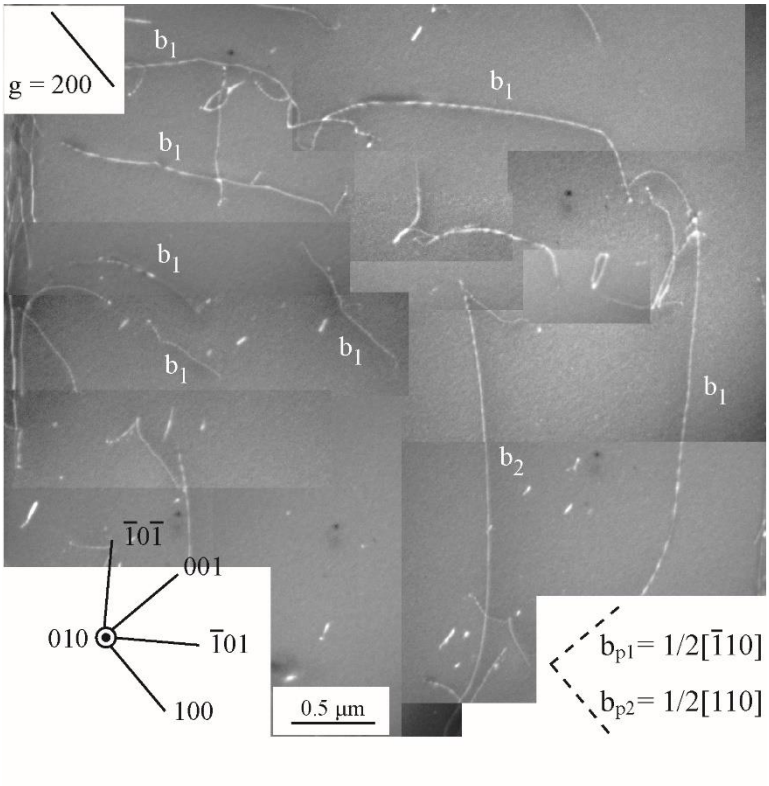

Fig. 6

Fig. 6: Ordinary dislocations in the (010) plane perpendicular to the tensile axis of the crept sample. b_P is the projection direction of the Burgers vector. (Thin foil: TFP2; Grain: 8).

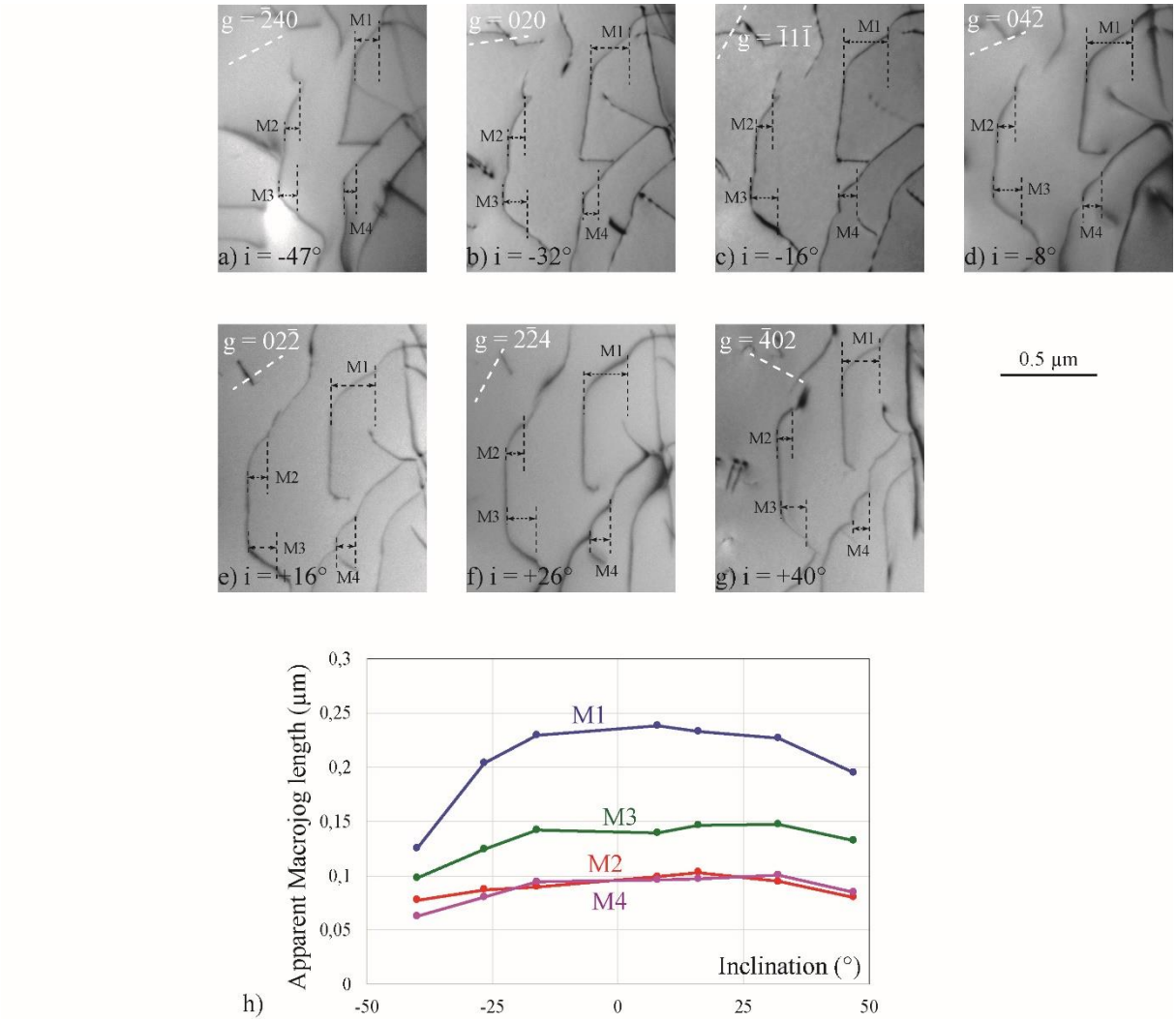

Fig. 7

Fig. 7: Tilt experiments on the area of Fig. 5 surrounded in blue. The width of four macrojogs is measured on each micrograph - (a) to (g). (h): variation of the apparent length of the macrojogs as a function of the inclination angle. (Thin foil: TFP1; Grain: 1).

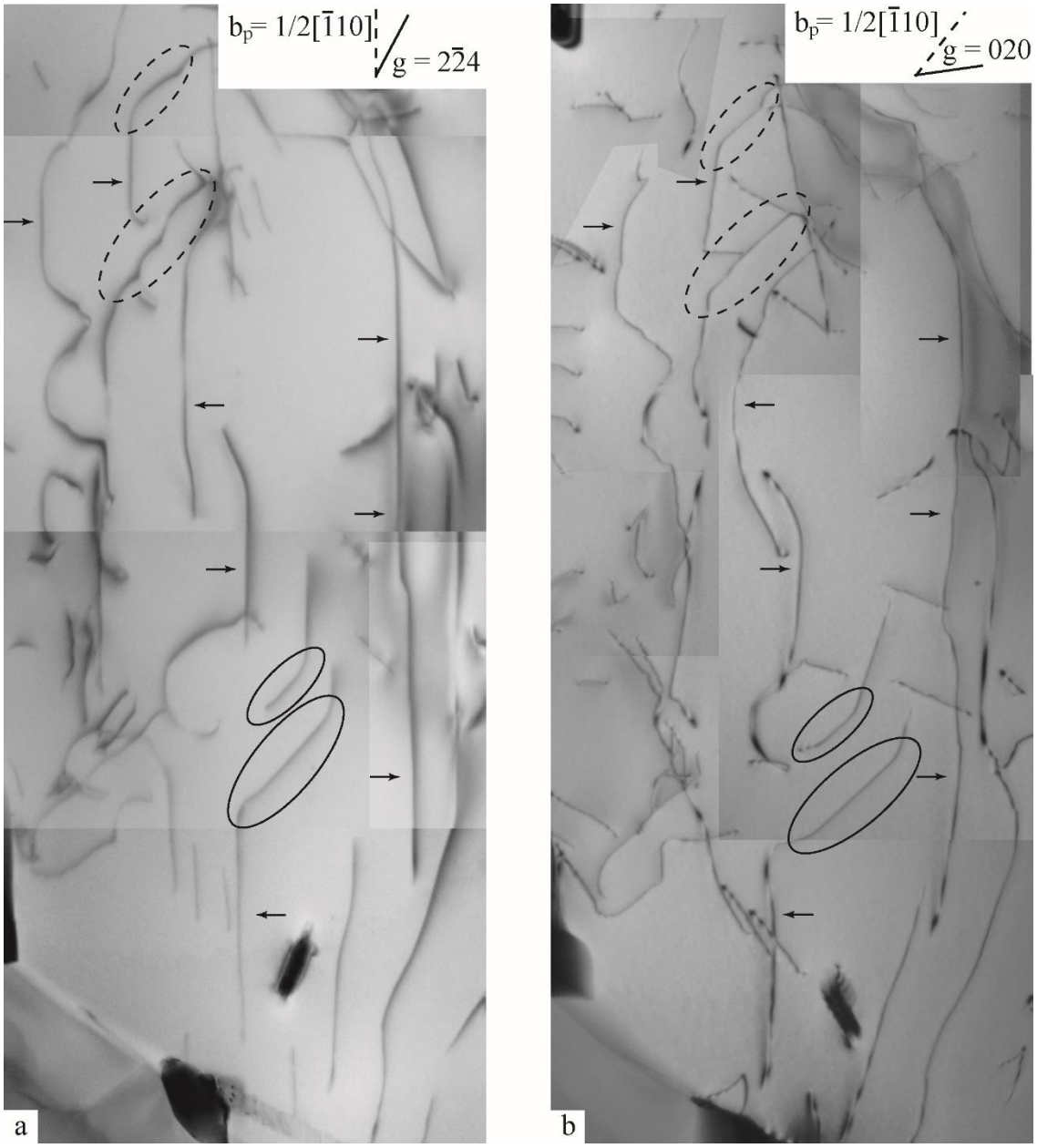

Fig. 8

Fig. 8: Views of the area of Fig. 5 under two inclinations for which the {111} type gliding planes of the dislocations are edge on. b_P is the projection direction of the Burgers vector. (Thin foil: TFP1; Grain: 1).

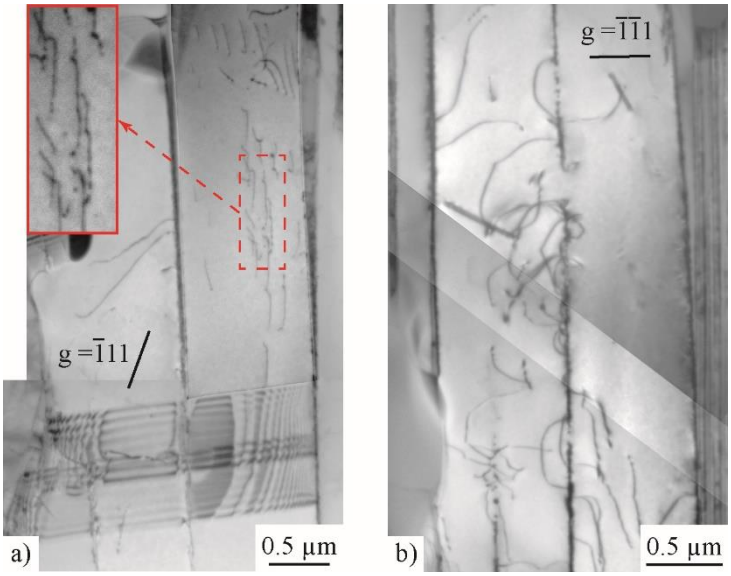

Fig. 9

Fig. 9: Examples of deformation microstructures in two lamellar zones.

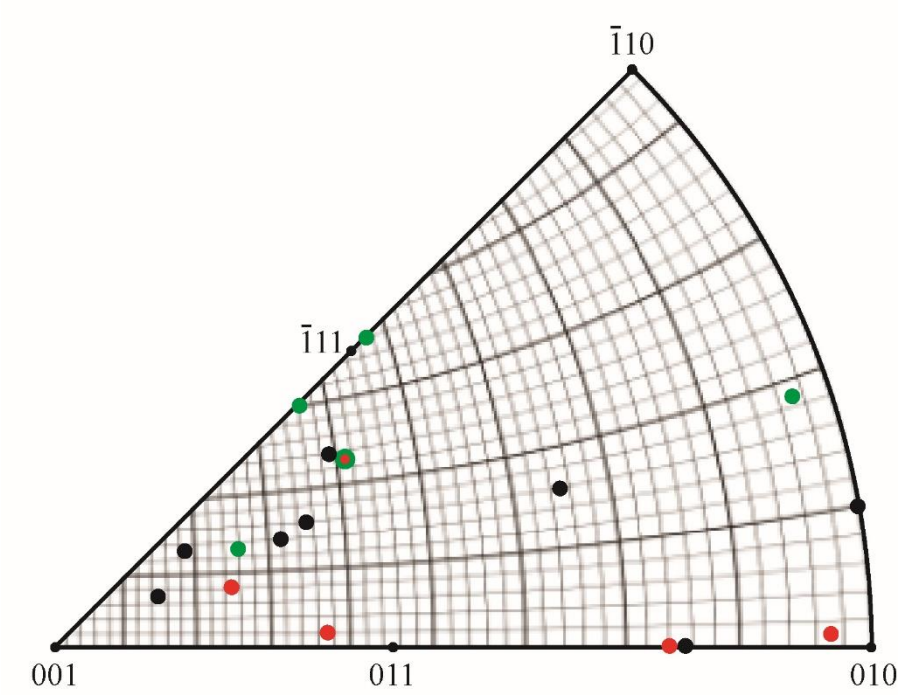

Fig. 10

Fig. 10: Standard triangle adapted to the $L1_0$ structure on which the loading axis of the 17 investigated γ grains have been reported. Points green and red indicates the grains addressed in Tab. 1, in which it has been unambiguously determined the activation of glide or climb, respectively.

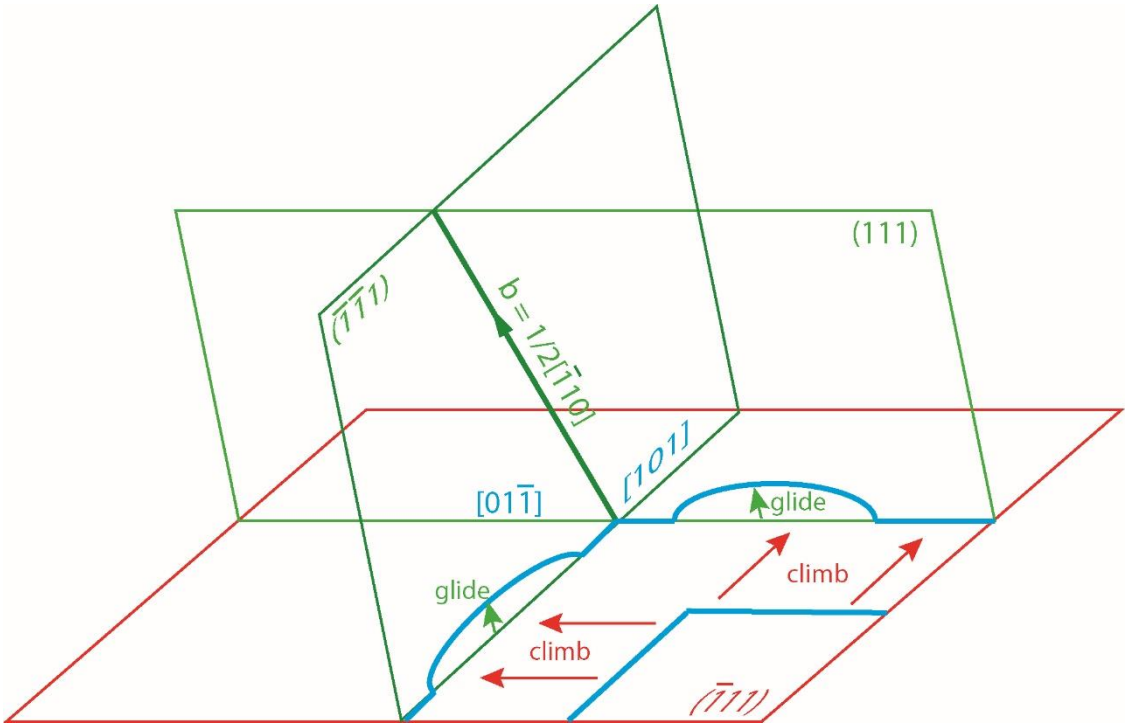

Fig. 11

Fig. 11: sketch of this climb processes and of the deviation of the sixty degrees' dislocations in the {111} planes, designed according to the situation studied in the Figs. 5, 7 and 8.